Mechanical properties of carbon nanotube networks by molecular mechanics and impact molecular dynamics calculations

V. R. Coluci,[1,*] S. O. Dantas,[1,2] A. Jorio,[3] and D. S. Galvão[1]
[1]*Instituto de Física "Gleb Wataghin," Universidade Estadual de Campinas, C.P. 6165, 13083-970 Campinas, São Paulo, Brazil*
[2]*Departamento de Física, ICE, Universidade Federal de Juiz de Fora, 36036-330 Juiz de Fora, Minas Gerais, Brazil*
[3]*Departamento de Física, Universidade Federal de Minas Gerais, Belo Horizonte 30123-970, Minas Gerais, Brazil*
(Received 19 September 2006; revised manuscript received 30 November 2006; published 16 February 2007)

We report a theoretical investigation of the mechanical properties of idealized networks formed by single-walled carbon nanotubes showing crossbar and hexagonal architectures. The study was performed by using molecular mechanics calculations and impact dynamics simulations based on bond-order empirical potential. The studied networks were predicted to have elasticity modulus of ~10–100 GPa and bulk modulus of ~10 GPa. The results show a transition from high to moderate flexibility during the deformation stages. This behavior was associated with the existence of two deformation mechanisms presented by the network related to the nanotube stretching and junction bending processes.

DOI: 10.1103/PhysRevB.75.075417 PACS number(s): 81.05.Uw, 81.05.Zx

I. INTRODUCTION

Carbon nanotubes are one of the most important materials for the development of nanotechnology. The use of such material can already be seen in various applications including field-emission displays, high-strength composites, hydrogen storage, and nanometer-sized semiconductor devices.[1,2] In the particular case of carbon nanotube based electronic devices, a breakthrough can be expected when the "bottom-up" manufacturing approach could be used in a controllable and self-assembled way. This would allow the fabrication of organized macroscale structures from nanoscale components. Among these organized structures are carbon nanotube networks.

Many attempts have been made in order to obtain carbon nanotube networks.[3–9] Exploring the high polarizability presented by single-walled carbon nanotubes (SWCNTs), Zhang *et al.*[3] have grown aligned nanotubes by chemical-vapor deposition coupled to electric-field application. Snow *et al.* have demonstrated the capacity of interconnected random networks of SWCNTs deposited on a substrate of functioning as thin-film transistors[4] and chemical sensors.[5] Single-walled carbon nanotube networks have also been fabricated on predefined substrate patterns[6] and on microcapsule arrays[7] by chemical-vapor deposition.

Most of the above-mentioned works have produced random networks, but more organized arrangements have also been obtained.[8,9] Diehl *et al.* have presented a room-temperature technique for assembling SWCNT ropes in the crossbar configuration by chemical control.[8] Exploring the morphologies of the SiC surfaces, Derycke *et al.* were able to produce catalyst-free horizontal carbon nanotube networks showing "hexagonal" and "crossbar" architectures.[9]

While organized networks consist mainly of ropes or bundles of SWCNTs,[8,9] recent achievements have shown the possibility of fabricating highly oriented isolated SWCNTs directly on top of substrate surfaces.[10–12] Ismach and Joselevich have demonstrated the formation of crossbar networks by simultaneously using graphoepitaxy and field-directed growth of SWCNTs by chemical-vapor deposition.[12] In those networks, the nanotube crossbar junctions are bonded by van der Waals interactions with the nanotubes radially deformed at the junctions. It has been experimentally observed[13] and theoretically investigated[14] that covalent bonds can be formed between two crossing SWCNTs when exposed to electron beam at high temperatures, forming a stable junction. The coupling of the steps previously mentioned can lead to the possibility of fabrication of isolated ordered covalently joined SWCNT networks. These networks could be considered as the ultimate arrangement involving SWCNTs, which are constructed by using "X-like," "Y-like," or "T-like" junctions.[13,15,16] The controlled fabrication of such networks can allow their use in applications such as sensors, filters, flexible electronic devices, composites, and electromechanical actuators. Three of us have used the idea of carbon nanotube networks to generate "super" carbon nanotubes.[17]

In this work, we present a theoretical investigation focusing on the mechanical properties of different SWCNT networks using molecular mechanics calculations and impact molecular dynamics simulations. While the former approach allows the determination of properties such as Young's and bulk modulus, the latter gives information about dynamical responses of the network to external colliding objects.

II. METHODOLOGY

Two types of SWCNT networks were considered: crossbar and hexagonal configurations. The networks are constructed using one single type of carbon nanotube connected by junctions being labeled as Cb@(n,m) and Hex@(n,m) for crossbar and hexagonal networks formed by (n,m) carbon nanotubes, respectively. The geometry of the junctions that connect carbon nanotubes is not unique. In this work, the tubes were connected using junctions constructed using five-membered and eight-membered rings[18] and five- and eight-membered rings[19] for (6, 0) and (8, 0) SWCNTs, respectively. Besides the nanotube type, the networks are characterized by the lengths a and b of the characteristic unit cell

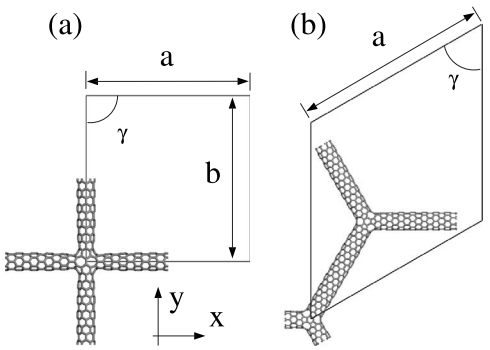

FIG. 1. Crossbar (a) and hexagonal (b) unit cells of isolated SWCNT networks. The crossbar net is made by (6, 0) while the hexagonal one by (8, 0) SWCNTs.

and by the angle γ, with $\gamma=90°$ and $\gamma=60°$ for crossbar and hexagonal networks, respectively. The choice of the specific values of a and b was arbitrary but limited by computational resources, which did not allow us to use unit cells with larger values. Some representative units of these networks are presented in Fig. 1. We also investigated multilayered networks formed by *AA*-stacking type of single layers as represented in Fig. 2. For comparative purposes, we also analyzed the graphite and a single graphite sheet (graphene). In this sense, the graphene is associated with the single layered networks and graphite to the multilayered ones.

The multilayered networks were initially optimized using the universal force field available on the software[21] CERIUS[2]. The optimizations were performed by varying both atomic coordinates and unit-cell parameters, with the exception of the α and β angles in order to produce multilayered networks (*AA*-stacking type in the z direction, Fig. 2). For the structures considered here, we have obtained the values of 8.3 and 9.4 Å for the unit-cell parameter c for the nets constructed with (6, 0) and (8, 0) SWCNTs, respectively. After geometrical optimization, the second derivatives of the lattice energy U with respect to the lattice parameters and the atomic coordinates were determined to obtain the elasticity tensor. When

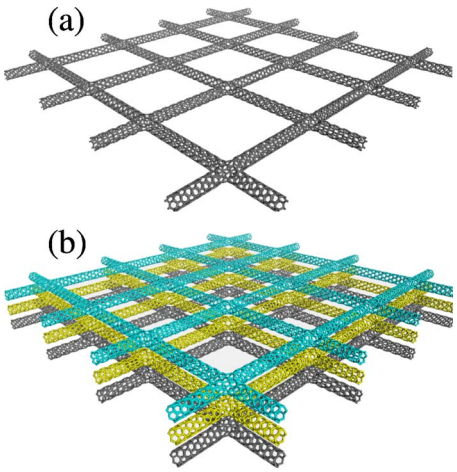

FIG. 2. (Color online) Representations of (a) a single layered and (b) multilayered (*AA* stacking) crossbar carbon nanotube network. Different colors represent different layers.

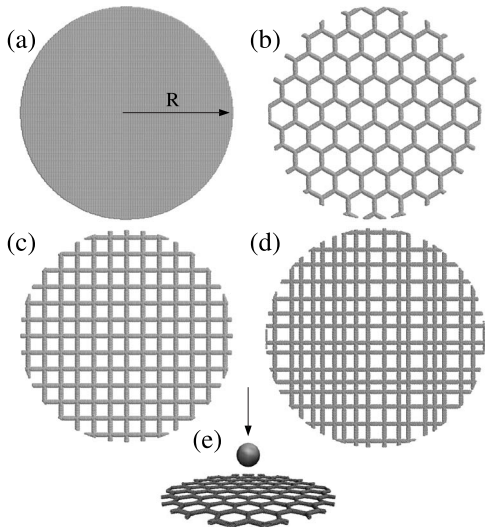

FIG. 3. Network models used in the impact molecular dynamics simulations. (a) A circular graphene sheet ($R=190$ Å), (b) a hexagonal [Hex@(6,0), $a=47.5$ Å], (c) a crossbar ($a=29.1$ Å and $b=29.9$ Å), and (d) a disordered network. (e) Representation of a spherical particle which will collide with the center of the network.

the structure is at an energy minimum, the stiffness matrix **C** elements can be obtained by $C_{ij}=\partial U^2/\partial\epsilon_i\partial\epsilon_j$, where ϵ is the strain. With the compliance matrix $\mathbf{S}=\mathbf{C}^{-1}$, we can obtain Young's (Y) and bulk (B) moduli as follows:

$$Y_x = 1/S_{11}, \quad Y_y = 1/S_{22}, \quad Y_z = 1/S_{33}, \tag{1}$$

and

$$B = 1/[S_{11} + S_{22} + S_{33} + 2(S_{31} + S_{21} + S_{32})]. \tag{2}$$

In order to study the dynamical behavior of the single layered networks, we have carried out impact molecular dynamics simulations considering cases until the rupture of the material was observed. For the cases where bond breaking and formation are important, standard molecular force fields (that often use quadratic form terms) are no longer suitable. Therefore, we have opted to use the adaptive intermolecular reactive empirical bond-order (AIREBO) potential developed by Stuart *et al.*[20] to model carbon-carbon interactions. AIREBO is similar to the reactive potential developed by Brenner,[22] but it incorporates by suitable modifications the nonbonded interactions through an adaptative treatment of the intermolecular interactions. This kind of reactive potential has been proven to be accurate in describing carbon nanotube deformations under mechanical strain.[23] The networks used in our impact studies have a circular target shape with radius $R=190$ Å, with the atoms at the outermost (width of ~5 Å) kept fixed during the simulations. The remaining regions are maintained at the temperature of 300 K by using the rescaling velocity method. We have used graphene sheet (44 553 atoms), Hex@(6,0) ($a=47.5$ Å, 25 376 atoms), and Cb@(6,0) ($a=29.1$ Å and $b=29.9$ Å, 39 259 atoms, and $a=16.5$ Å and $b=17.4$ Å, 63 340 atoms) networks (Fig. 3) as targets for a spherical (radius of 50 Å) rigid particle with initial kinetic energy K_i and mass of 10% of the graphene sheet (53 463.6 amu), which collides with

the center of the networks [Fig. 3(e)]. The initial kinetic energy of the incident particle ranges from 1 to 10 keV corresponding to speed values of approximately 1900 to 6000 m/s. Such high speeds were needed to deform the networks, since they are very massive compared to the colliding particle. Simulations with lower speeds were done but showed no significant network deformation for the chosen value of the incident particle mass.

Despite the fact that our focus in the present work is on ordered networks, we also present results for a disordered system. The study of disordered networks deserves a separate work, since many aspects have to be analyzed, for instance, the distribution of the lengths (mean value and variance) of the nanotubes that constitute the networks, different junction arrangements, nanotube diameter distribution, and presence of defects (e.g., vacancies). We limited ourselves here to show only the results for the case where the nanotube lengths can be different in both in-plane network directions. Further and more detailed investigations of disordered systems are needed and are currently in progress. The disordered network investigated contains 48 291 carbon atoms and was generated by randomly distributing the lengths of the carbon nanotubes along the x and y directions [Fig. 3(d)].

The interaction between the incident particle of mass m and a carbon atom was modeled by the Lennard-Jones (LJ) 12-6 potential:

$$V^{\mathrm{LJ}}(r) = 4\epsilon\left[\left(\frac{\sigma}{r-r_0}\right)^{12} - \left(\frac{\sigma}{r-r_0}\right)^{6}\right], \quad r > r_0, \qquad (3)$$

where r is the distance between a carbon atom and the center of the spherical rigid particle of radius r_0. The parameters ϵ=5.42 meV and σ=3.4 Å were used.[24]

III. RESULTS AND DISCUSSIONS

The elastic properties of some multilayered carbon nanotube networks calculated using the universal force field[21] are presented in Table I. For comparison, we also present the values for graphite. The experimentally reported elastic constants of graphite depend on sample quality and measurement processes and present a large spread (see discussion in Ref. 26). Measurements using ultrasonic, sonic resonant, and static test methods, performed by Blasklee *et al.*[27] for compression-annealed pyrolytic graphite, resulted to a Young's modulus parallel and normal to the basal planes of 1.02 TPa and 36 GPa, respectively, and a bulk modulus of 36 GPa. The universal force field seems to overestimate the bulk modulus and to underestimate the basal plane Young's modulus by 20%, but it should be stressed that the model assumes perfect crystalline structures.

We can see from Table I that crossbar networks present in-plane Young's modulus (Y_x and Y_y) larger than ones presented by hexagonal networks by a factor of ~10 for comparable values of the distance between junctions. These values can be compared with the typical values for nylon (2–4 GPa), titanium (105–120 GPa), and steel (190–210 GPa). Furthermore, crossbar networks present different values for Young's modulus for in-plane directions.

TABLE I. Calculated Young's modulus (Y) and bulk modulus (B) of multilayered carbon nanotube networks and graphite. N_a is the number of atoms in the unit cell.

Structure	a (Å)	b (Å)	Y_x (GPa)	Y_y (GPa)	Y_z (GPa)	B (GPa)	N_a
Hex@(6,0)	40.0		22	22	15	14	364
	54.6		10	10	10	10	508
	61.9		7	7	9	8	580
Hex@(8,0)	42.8		44	44	13	13	504
	57.4		21	21	9	9	696
	72.0		12	12	7	7	888
Cb@(6,0)	16.5	17.4	280	324	36	35	156
	29.1	29.9	194	212	18	18	300
	37.5	38.4	162	173	14	14	396
	45.9	46.8	139	147	11	11	492
Graphite	2.6		799	799	47	43	4

For instance, Young's modulus for the crossbar network Cb@(6,0) (a=37.5 Å and b=38.4 Å) are 162 and 173 GPa for the x and y directions, respectively. This asymmetry in the mechanical properties is more pronounced for smaller a and b values. This is a result of the junction type used in the network construction. While X junctions used here for building crossbar networks present a C_2 symmetry, the Y junctions of the hexagonal networks show a C_3 one. These symmetry types are due to use of combinations of pentagons and heptagons, and pentagons and octagons, respectively.

For out-of-plane Young's modulus (Y_z), the values between the networks considered here are approximately the same and have the typical value of 10 GPa. Both in-plane and out-of-plane Young's moduli decrease with the increase of the distance between junctions (related to the parameters a and b). This trend can be associated with the high flexibility presented by SWCNTs that form the network sides (crossbar and hexagonal arrangements). For smaller values of a and b, the junctions are stiffer than in the case of larger values; therefore, the network presents a small flexibility. The small values of Y_z predicted for the networks are due to the large compressibility shown by SWCNTs when compressive stress is applied perpendicularly to the axial axis. These results indicate that the single-walled carbon nanotube networks investigated here are very flexible, showing smaller values of Young's and bulk moduli than graphite. This property has been experimentally observed in random networks[28] and can lead to important and useful features (as robustness under bending) that are helpful to flexible electronic devices.

Besides the static calculations based on molecular mechanics to obtain bulk mechanical properties (Table I) of the networks, it is important to foresee how these systems behave when subject to the action caused by the impact of an external object. In the present work, we performed impact molecular dynamics simulations to study the collision of an energetic particle to the networks. Firstly, we investigated the dependence of the incident particle characteristics on the dy-

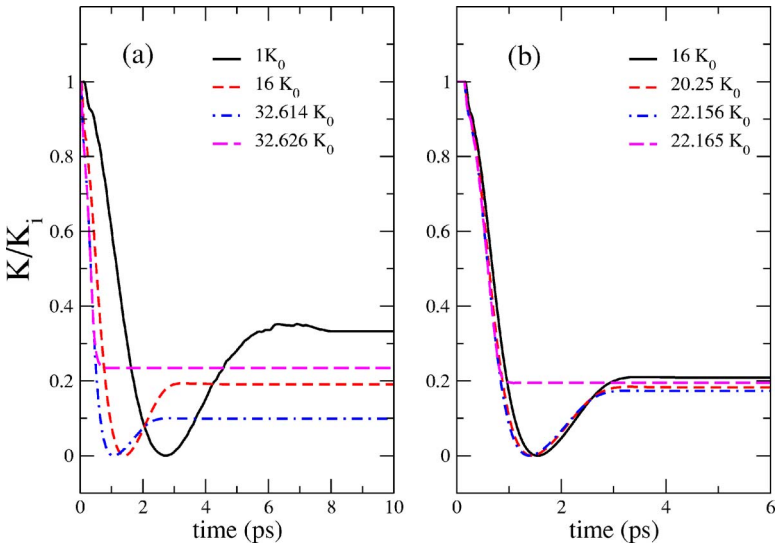

FIG. 4. (Color online) Temporal evolution of the kinetic energy K of the incident particle for different values of K_i (initial kinetic energy) for (a) $r_0=15$ Å and (b) $r_0=10$ Å. The particle mass is the same for both cases and it equals 15% of the graphene sheet mass. In this figure, $K_0 \equiv 211$ eV and the target is a squared graphene sheet. The necessary time for the particle to interact with the target depends upon the particle mass and radius as seen in (b) on the early stages of the simulation.

namical behavior of the networks by using a squared graphene sheet of 238 Å side length (22 572 atoms) as the target for incident particles with distinct radii, masses, and initial velocities. Figure 4 shows the temporal evolution of the kinetic energy K of the incident particle, normalized by its initial kinetic energy K_i ($t=0$), as it interacts with the graphene sheet for different K_i and particle radius r_0. As the particle impacts the target, it transfers its kinetic energy to the layer that absorbs it as stored elastic energy, vibrational modes, and part is also dissipated with the thermal effects. After the particle is stopped (with no rupture of the net), it is reflected backward with lower kinetic energy.

From Figs. 4(a) and 4(b), we can see that the general trends are the same, but the impact for the particle of larger radius [Fig. 4(a)] is more sensitive to the values of the particle kinetic energy. The rupture happens when K_i reaches the value K_r (necessary kinetic energy of the particle to cause the rupture of the layer), which is shown to be when K_i is approximately equal to 8150 eV (38.626 K_0) and 4677 eV (22.165 K_0) in Figs. 4(a) and 4(b), respectively [see complementary material, video01 (Ref. 29)]. The value of K_r is dependent of the particle size and mass as shown in Fig. 5. Smaller particles (smaller radius) need smaller energy to cause the rupture due to the higher stress applied in the layer. This fact is associated with the number of carbon bonds that the incident particle interacts with and the necessary energy to cause bond stretching and angle bending deformations. Since the incident particle is spherical, the number of bonds does not grow linearly as the particle radius.

The impact dynamics was then repeated to single layers of crossbar and hexagonal networks in order to estimate their elastic robustness under impact (Fig. 3). The results are compared with similar simulations with a graphene sheet as the target. Figure 6 shows the temporal evolution of the kinetic energy K of the incident particle normalized by its initial energy K_i when it collides with different networks. The values considered for K_i are smaller than the corresponding K_r of the investigated networks. The following typical behavior is seen in Fig. 6. The particle is initially retarded by the network until it rests and then pushed away until completely losing the contact with the network [see complementary material, video02–04 (Ref. 29)]. The reflected mechanical wave can make the incoming particle to assume a high energy due to a big displacement caused at the center of the network [see Fig. 6(a) for $K_i=10$ keV]. This effect would be relevant if the networks were suspended over patterns with typical sizes of 50 nm (for the size, mass, and speeds of the incoming particle considered here) as the ones constructed by soft lithography.[30] On the other hand, for even larger networks, the mechanical wave travels out and does not come back before the particle has been totally pushed back. The necessary time to completely stop the incident particle depends upon its initial energy as well as the network type. While for the graphene sheet the particle is rapidly pushed away by the network [Fig. 6(c)], for the hexagonal and crossbar networks, the particle spends a longer time in this situation, especially for higher incident energies. Furthermore, the colliding particle final kinetic energy (after losing contact with the target) for the same K_i is larger for the hexagonal network. This is

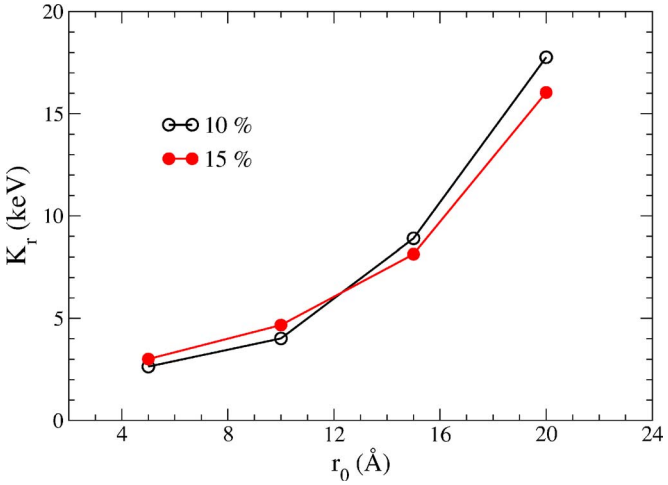

FIG. 5. (Color online) Necessary kinetic energy of the incident particle to cause the rupture of the graphene sheet. Results for two different particle masses are shown (10% and 15% of graphene sheet mass).

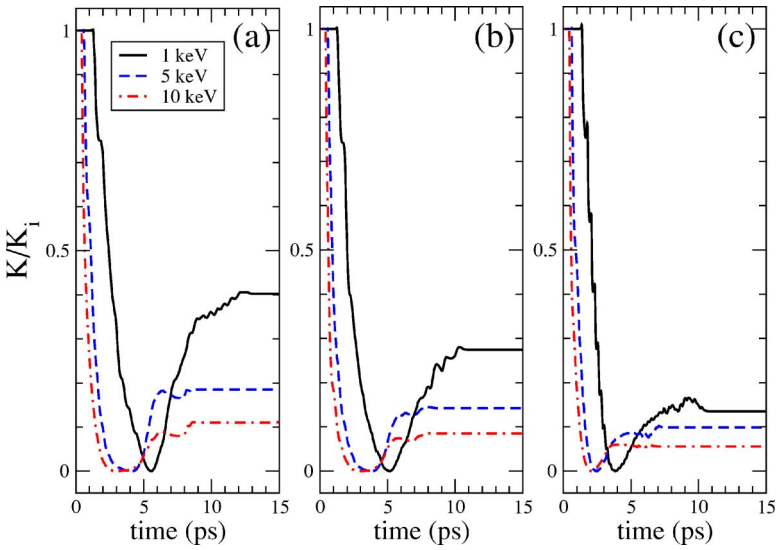

FIG. 6. (Color online) Temporal evolution of the kinetic energy K of the incident particle colliding with (a) a hexagonal network [Hex@(6,0), a=47.5 Å], and (b) crossbar network (a=29.1 Å and b=29.9 Å), and (c) a graphene sheet.

an indication that this material would dissipate less energy through phonons and to thermal effect. These results reflect the larger flexibility presented by the crossbar and hexagonal networks when compared to a single graphene sheet (see Table I).

A typical response of the networks is shown in Fig. 7 through various snapshots of the impact of a 5 keV particle with a crossbar network. The collision causes a local deformation on the network, generating a shock wave that propagates through it. At 2.5 ps, the particle is almost stopped and the deformation caused in the network propagates until approximately 4.5 ps when the shock wave reaches the borders and it is reflected. At approximately 5 ps, the particle begins to be accelerated backward by the network during about 1.5 ps when then, at about 9 ps, it completely loses contact with the network.

In order to see the temporal evolution of the energy spreading through the network, we have determined the local temperature as a function of time. The local "temperature" of an atom was obtained by the mean squared velocity of the neighboring atoms inside a local volume delimited by a sphere of radius of 5 Å.[31] Figure 8 shows the temperature profiles for the simulation of Fig. 7. An increase of the local temperature is seen near the impact region (Fig. 8, 2.5 ps) reaching up to 630 K. While the central region (collision) remains "hot" (4 ps), the energy is gradually spread out through the network. The formation of "cool" regions (5 ps) that also propagate (9 ps) is observed.

The network responses to the colliding particle are analyzed by looking at the normal deformation (Δz) of the network calculated as the displacement of the particle from the point where it begins to interact with the network until the one when the particle is completely stopped by it. Figure 9 presents the behavior of $(\Delta z)^2$ as a function of the initial kinetic energy of the incident particle. The data can be fitted by the expression $(\Delta z)^2 \propto K^{\beta}$, where β corresponds to the inclination of the curves. For the graphene sheet, a single value of β is sufficient to represent the data, at least in the range of the investigated initial kinetic energies. On the other hand, two different values are necessary for the nanotube networks. Larger values fit the behavior for lower-initial-

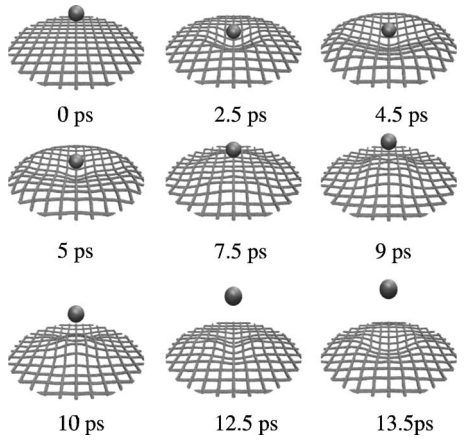

FIG. 7. Snapshots of the impact of a 5 keV particle with a crossbar network [Cb@(6,0), a=29.1 Å, b=29.9 Å].

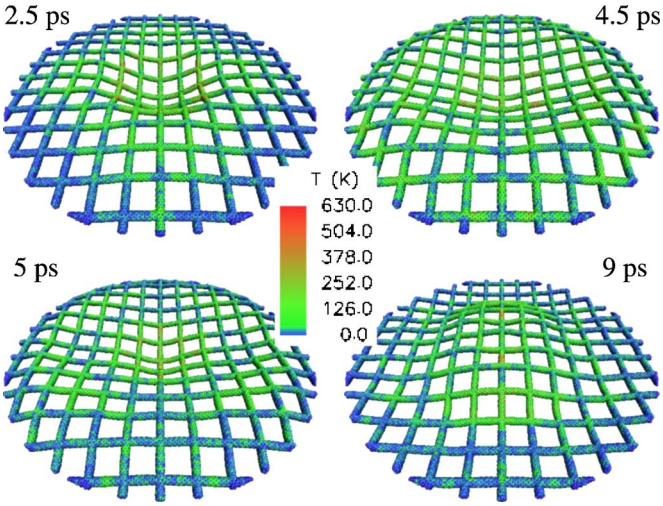

FIG. 8. (Color online) Temperature profile for different times of the simulation of the collision of a 5 keV particle on the crossbar network (Fig. 7).

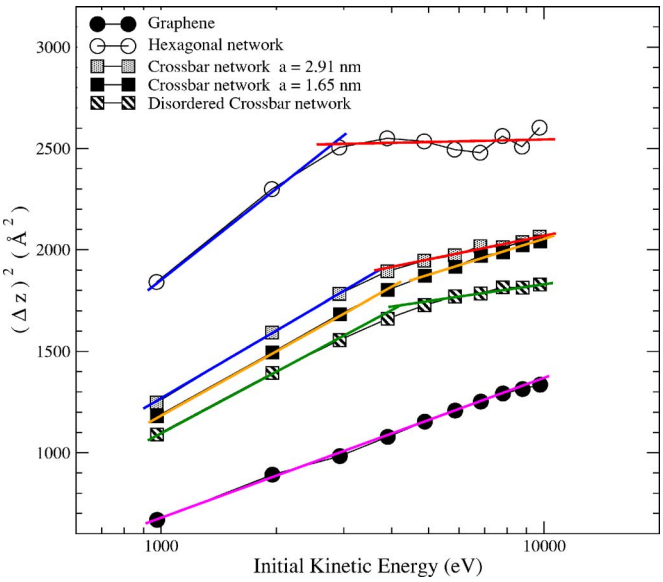

FIG. 9. (Color online) Behaviors of the squared normal deformation $(\Delta z)^2$ as a function of the initial kinetic energy of the incident particle. The targets are the ones shown in Fig. 3. The colored lines are only to help visualization of the different regimes.

energy regions ($\lesssim$2.7 and $\lesssim$3.5 keV for the ordered hexagonal and crossbar networks, respectively), while smaller ones to the behavior for higher energies.

These two different behaviors, associated with two different values of β, suggest the existence of different response mechanisms. We named them bending and stretching mechanisms, where for each of them a spring constant could be associated. The former is associated with changes of the angle γ formed by nanotubes and the junction (γ=90° and γ=60° for ordered crossbar and hexagonal networks, respectively). The stretching regime is related to the axial stretching of the SWCNTs that form the network. For the low-incident-energy regime, the main contribution to the deformation of the network would be caused by the bending mechanism. On the other hand, for the high-energy regime, when the angle deformation is maximum (dictated by the network geometry), it is the stretching mechanism that is responsible for the main behavior of the network. Since SWCNTs present a high Young's modulus in the axial direction, it is reasonable to assume that the spring constant associated with the stretching mechanism would be larger than the one related to the bending one. Thus, it would be more difficult to change the position of the incident particle in the stretching regime as observed in the simulations (Fig. 6). This can be easily seen in the behavior of the hexagonal network (Fig. 9). However, it is worth noting that the values of β as well as $(\Delta z)^2$ would depend upon the network type, dimensions, and sheet shapes (circular in our case). Nevertheless, the presence of two regimes is still expected once the extremities of the network are kept fixed, e.g., suspended networks. The changes in the β and $(\Delta z)^2$ values can be seen when we analyze networks with a different geometry, e.g., crossbar networks. In these cases, we can see that the two slopes are also present. However, the difference between them is not as evident as in the case of the hexagonal network. Furthermore, when the amount of network void space (porosity) is diminished, i.e., by decreasing the a and b values, the difference is even smaller, tending to the situation of a network without porosity (graphene sheet). The same trend is expected for hexagonal networks. These results indicate that the separation between the stretching and bending mechanisms is more pronounced when the network porosity is larger.

The presence of disorder in the network also changes the response behavior. This is seen for the case of the disordered crossbar network generated here by randomly distributing the carbon nanotube lengths and thus causing a not regular distribution of the network porosity. For the disordered network investigated here, similar behaviors (not shown here) of the evolution of the incident particle kinetic energy (Fig. 7) to the ordered cases were observed. However, while the decrease of network porosity leads to an increase of β for the high-energy region, a disordered porosity produces a decrease of it.

The existence of these well-defined regimes suggests that the networks would present a high flexible behavior for small deformations perpendicularly applied to the network surface but would reach a less flexible state for larger deformations. Changing the network characteristics (architecture, nanotube type, unit-cell dimensions, disorder) would tune the main mechanism type and, consequently, the mechanical properties presented by the network.

It has been experimentally observed that the electronic properties of carbon nanotubes can be altered by mechanical strain.[32] In this sense, suspended carbon nanotube networks can also have their transport and even optical properties changed by normal deformation. Furthermore, due to the elastic properties predicted for the networks, they can support large elastic deformations, which can lead to measurable changes in electronic quantities. By quantifying these changes, one could determine the normal displacement and/or the velocity of incident nanoparticles.

IV. CONCLUSIONS

The elastic properties of single-walled carbon nanotube networks were investigated by molecular mechanics calculations and impact dynamics simulations. Our results showed that they exhibit very high flexibility dependent on the network architectures, showing elasticity modulus of $\sim$10–100 GPa and bulk modulus of $\sim$10 GPa. Due to the construction of the network involving SWCNTs and junctions, different response mechanisms under normal deformation for suspended networks are expected. They are associated with carbon nanotube stretching and nanotube-junction-nanotube angle bending, which contribute differently depending on the degree of deformation of the network. The symmetry presented by the junctions that constitute the network and the network disorder are important aspects on the resulting mechanical properties. Exploiting the demonstrated capability of carbon nanotubes of having changed their electronic properties under strain, carbon nanotube networks could be used as position detecting devices.

Our results also suggest that it is possible to tune the elastic properties of the structures by varying the tube length and type as well as the network architecture. The impact molecular dynamics simulations also indicated that these materials would exhibit very interesting properties as impact absorbing structures. The rapid evolution of the synthetic methods recently observed for carbon nanotube networks might lead to the experimental realization of the here proposed structures.

ACKNOWLEDGMENTS

We acknowledge the financial support from the Instituto de Nanotecnologia/CNPq, Rede de Nanotubos/CNPq, and IMMP/CNPq, and the Brazilian agencies FAPESP, FAPEMIG, Capes, and CNPq. V.R.C. and D.S.G. thank Susan B. Sinnott for helpful discussions. The authors also would like to thank Steven J. Stuart for generously providing us with the force and energy routines for AIREBO potential.

*Author to whom correspondence should be addressed. FAX:+55-19-35215343. Electronic address: coluci@ifi.unicamp.br

[1] R. Saito, G. Dresselhaus, and M. S. Dresselhaus, *Physical Properties of Carbon Nanotubes* (Imperial College Press, London, 1998).
[2] R. H. Baughman, A. A. Zakhidov, and W. A. de Heer, Science **297**, 787 (2002).
[3] Y. Zhang, A. Chang, J. Cao, Q. Wang, W. Kim, Y. Li, N. Morris, E. Yenilmez, J. Kong, and H. Dai, Appl. Phys. Lett. **79**, 3155 (2001).
[4] E. S. Snow, J. P. Novak, P. M. Campbell, and D. Park, Appl. Phys. Lett. **82**, 2145 (2003).
[5] E. S. Snow, J. P. Novak, M. D. Lay, E. H. Houser, F. K. Perkins, and P. M. Campbell, J. Vac. Sci. Technol. B **22**, 1990 (2004).
[6] Y. J. Jung, Y. Homma, T. Ogino, Y. Kobayashi, D. Takagi, B. Wei, R. Vajtai, and P. M. Ajayan, J. Chem. Phys. **107**, 6859 (2003).
[7] A. M. Cassel, G. C. McCool, H. T. Ng, J. E. Koehne, B. Chen B, J. Li, J. Han, and M. Meyyappan, Appl. Phys. Lett. **82**, 817 (2003).
[8] M. R. Diehl, S. N. Yaliraki, R. A. Beckman, M. Barahoma, and J. R. Heath, Angew. Chem. **114**, 363 (2002).
[9] V. Derycke, R. Martel, M. Radosavljevic, F. M. Ross, and Ph. Avouris, Nano Lett. **2**, 1043 (2002).
[10] H. Ago, K. Nakamura, K. Ikeda, N. Uehara, N. Ishigami, and M. Tsuji, Chem. Phys. Lett. **408**, 433 (2005).
[11] A. Ismach, D. Kantorovich, and E. Joselevich, J. Am. Chem. Soc. **127**, 11554 (2005).
[12] A. Ismach and E. Joselevich, Nano Lett. **6**, 1706 (2006).
[13] M. Terrones, F. Banhart, N. Grobert, J. C. Charlier, H. Terrones, and P. M. Ajayan, Phys. Rev. Lett. **89**, 075505 (2002).
[14] I. Jang, S. B. Sinnott, D. Danailov, and P. Keblinski, Nano Lett. **4**, 109 (2004).
[15] L. P. Biro, Z. E. Horvath, G. I. Mark, Z. Osvath, A. A. Koos, A. M. Benito, W. Maser, and P. Lambin, Diamond Relat. Mater. **13**, 241 (2004).
[16] M. Terrones, Annu. Rev. Mater. Res. **33**, 419 (2003).
[17] V. R. Coluci, D. S. Galvão, and A. Jorio, Nanotechnology **17**, 617 (2006).
[18] I. Zsoldos, G. Kakuk, T. Reti, and A. Szasz, Modell. Simul. Mater. Sci. Eng. **12**, 1251 (2004).
[19] D. Srivastava, S. Saini, and M. Menon, Ann. N.Y. Acad. Sci. **852**, 178 (1998).
[20] S. J. Stuart, A. B. Tutein, and J. A. Harrison, J. Chem. Phys. **112**, 6472 (2000).
[21] UFF-Universal1.02 molecular force field in CERIUS^2 program, Accelrys, Inc., http://www.accelrys.com
[22] D. W. Brenner, Phys. Rev. B **42**, 9458 (1990); **46**, 1948 (1992); D. W. Brenner, J. A. Harrison, C. T. White, and C. T. Colton, Thin Solid Films **206**, 220 (1991).
[23] B. I. Yakobson, C. J. Brabec, and J. Bernholc, Phys. Rev. Lett. **76**, 2511 (1996).
[24] The LJ parameters are given by $\epsilon=\sqrt{\epsilon_C\epsilon_{Ar}}$ and $\sigma=(\sigma_C+\sigma_{Ar})/2$, where C and Ar refer to carbon and argon, respectively, with $\epsilon_{Ar}=10.3$ meV, $\sigma_{Ar}=3.41$ Å (Ref. 25), and $\epsilon_c=2.84$ meV, $\sigma_c=3.4$ Å (Ref. 20). We have arbitrarily chosen the parameters of argon to represent the incident particle.
[25] A. Michels, H. Wijker, and H. K. Wijker, Physica (Amsterdam) **15**, 627 (1949).
[26] A. Krishnan, E. Dujardin, T. W. Ebbesen, P. N. Yianilos, and M. M. J. Treacy, Phys. Rev. B **58**, 14013 (1998).
[27] O. L. Blakslee, D. G. Proctor, and E. J. Seldin, J. Appl. Phys. **41**, 3373 (1970).
[28] S-H. Hur, O. O. Park, and J. A. Rogers, Appl. Phys. Lett. **86**, 243502 (2005).
[29] See EPAPS Document No. E-PRBMDO-75-070711 for movies, in MPG format, of simulations discussed in the paper. For more information on EPAPS, see http://www.aip.org/pubservs/epaps.html.
[30] T. A. Von Werne, D. S. Germack, E. C. Hagberg, V. V. Sheares, C. J. Hawker, and K. R. Carter, J. Am. Chem. Soc. **125**, 3831 (2003).
[31] M. Keford and R. P. Webb, Carbon **37**, 859 (1999).
[32] E. D. Minot, Y. Yaish, V. Sazonova, J. Y. Park, M. Brink, and P. L. McEuen, Phys. Rev. Lett. **90**, 156401 (2003).